Supporting Information

Electrochemical Activation of Heterometallic Nanofibers for Hydrogen Evolution

Yali Xiao, Hao Yang, Xi Gong, Lei Hu, Yexiang Tong* and Jianyong Zhang*

Sun Yat-Sen University, MOE Laboratory of Polymeric Composite and Functional Materials, School of Materials Science and Engineering, School of Chemistry, Guangzhou 510275, China.

Corresponding Author

* zhjyong@mail.sysu.edu.cn (J. Z.); chedhx@mail.sysu.edu.cn (Y. T.).

Materials and Characterization

Chemicals and solvents were obtained from commercial sources and used as received without further purification unless otherwise stated. $Pd(COD)Cl_2$ (COD = 1,5-cyclooctadiene) was synthesized according to the previous report.[1] Scanning electron microscopy (SEM) was performed using an ultra-high resolution Quanta 400F-SEM (FEI, working voltage is 20 kV, working current is 10 μA). Prior to SEM measurements, the material was dispersed in ether with the aid of sonication, and then deposited on aluminium foil. Transmission electron microscopy (TEM) investigations were carried out on a FEI Tecnai G2 F30 TEM system. The sample was dispersed in ether and mounted on a copper grid. Powder X-ray diffraction (XRD) data was collected on a D-MAX 2200 VPC diffractometer (Bragg-Brentano geometry, Cu-Kα1 radiation, λ = 1.54056 Å). IR spectra and Raman spectra were measured on the Bruker Tensor 27 Fourier transform infrared spectrometer and Laser Micro-Raman Spectrometer, respectively, which scanning range is 400~4000 cm^{-1}. Nexsa X-ray photoelectron spectrometer (XPS) system was used to analyze the xerogel elements and their changes in binding energy. The N_2 adsorption/desorption test was performed on the Quantachrome autosorb-iQ2 analyzer. Prior to the test, the sample was heated at 80 °C under vacuum for 16 h, supplemented with He under normal pressure, and then adsorbed for N_2 at 77 K.

Table S1. Gelation tests of the **Pd-M** system with various transition metal ions and rare earth metal ions.

Metal salt	Result	Color	Time
$NiCl_2·6H_2O$	gel	yellowish green	30-40 min
$Ni(NO_3)_2·6H_2O$	gel	yellow	30-40 min
$CoCl_2·6H_2O$	gel	dark green	30-40 min
$Co(NO_3)_2·6H_2O$	gel	indy pink	30-40 min
$CuCl_2·2H_2O$	gel	yellowish green	30-40 min
$MnCl_2$	gel	light yellow	ca. 30 min
$Mn(NO_3)_2$	gel	yellow	ca. 30 min
$Al(NO_3)_3·9H_2O$	gel	yellow	6 d
$Fe(NO_3)_3·9H_2O$	solution	reddish brown	-
$FeCl_3$	gel	reddish brown	ca. 30 min
$Cr(NO_3)_3·9H_2O$	solution	blue gray	-
$ZnCl_2$	gel	light yellow	30-40 min
$Y(NO_3)_3·6H_2O$	gel	light yellow	ca. 30 min
$Tb(NO_3)_3·6H_2O$	gel	light yellow	ca. 30 min
$La(NO_3)_3·6H_2O$	gel	light yellow	ca. 30 min
$Ce(NO_3)_3·6H_2O$	gel	light yellow	ca. 30 min

Reaction conditions: 0.04 mmol of pyridine-3,5-dicarboxylic acid, 0.02 mmol of $Pd(COD)Cl_2$ and 0.04 mmol of metal salt were used for gelation tests.

Table S2. Gelation tests of the **Pd-Ni** system in various solvents.

Solvent	Result	Time
DMF-MeCN-MeOH	gel	ca. 30 min
DMF-MeCN-H_2O	ppt	/
DMF-MeCN	gel	ca. 40 min
DMF-MeOH	gel	ca. 20 min
DMF-H_2O	weak gel	ca. 20 min
DMF	solution	/
DMSO-MeCN-MeOH	solution	/
DMSO-MeCN-H_2O	solution	/
DMSO-MeOH	solution	/
DMSO-H_2O	solution	/
DMSO	solution	/
DMA-MeCN-MeOH	gel	ca. 2 h
DMA-MeCN-H_2O	gel	ca. 2 h
DMA-MeCN	solution	/
DMA-H_2O	solution	/
DMA	solution	/

Reaction conditions: 0.04 mmol of pyridine-3,5-dicarboxylic acid, 0.02 mmol of $Pd(COD)Cl_2$ and 0.04 mmol of $NiCl_2{\cdot}6H_2O$ were used for gelation tests.

Table S3. Gelation tests of the **Pd-Ni** system in various concentrations.

Entry	DMF/μL	MeCN/μL	MeOH/μL	H_2O/μL	c/(mmol L^{-1})[a]	Result	Time
1	800	500	0	200	13.3	gel	30 min
2	800	500	200	0	13.3	gel	30 min
3	1000	500	400	100	10	gel	30-40 min
4	800	600	600	0	10	gel	30 min
5	800	600	800	0	9.1	gel	30-40 min
6	1000	600	600	0	9.1	gel	30-40 min
7	1000	800	700	0	8	gel	30-40 min
8	1200	800	800	200	6.7	solution	/
9	1500	1000	1000	500	5	solution	/

Reaction conditions: 0.04 mmol of pyridine-3,5-dicarboxylic acid, 0.02 mmol of $Pd(COD)Cl_2$ and 0.04 mmol of $NiCl_2{\cdot}6H_2O$ was used for gelation. [a] Based on Pd^{2+}.

Table S4. N_2 adsorption/desorption tests of bimetallic **Pd-M** xerogels.

Material	S_{BET}/m^2 g^{-1}	V_{total}/cm^3 g^{-1}	V_{micro}/cm^3 g^{-1} [a]	V_{meso}/cm^3 g^{-1} [b]
Pd-Co	20.0	0.139	0.009	0.12
Pd-Ni	14.4	0.0941	0.004	0.083
Pd-Mn	14.3	0.0486	0.007	0.045

[a] V_{micro} was calculated by the SF method, [b] V_{meso} was calculated by the BJH method.

Table S5. HER catalytic activities of **Pd-M** xerogels loaded on GCE.

Material	E_{onset} (mV)	overpotential at 10 mA cm^{-2} (mV)	Tafel slope (mV dec^{-1})
Pd-Co	69	188	60
Pd-Ni	117	224	66
Pd-Mn	131	263	189
Pd	131	263	91
Pt/C	35	58	42

Table S6. HER catalytic activities of **Pd-M** xerogels loaded on NF.

Material	E_{onset} (mV)	overpotential at 10 mA cm^{-2} (mV)	overpotential at 50 mA cm^{-2} (mV)	Tafel slope (mV dec^{-1})
EA Pd-Co@Pd NPs-NF	44	57	96	55
Pd-Co-NF	37	96	172	63
Pd-Ni-NF	48	107	174	69
Pd-Mn-NF	72	132	199	88
Pd-NF	52	137	215	75
Pt/C	34	57	135	42
NF	318	417	/	/

Each loading amount of Pd-M xerogels was 3.5 mg cm^{-2} in average and the loading amount of 20% Pt/C was 3.2 mg cm^{-2}.

Table S7. Comparison of HER activity among recently reported various electrocatalysts.

Material	Overpotential at 10 mA cm^{-2} (mV)	Tafel slope (mV dec^{-1})	Conductive substrate	Structure	ref
NiFeP	178	69	GCE	nanorod-like	[2]
FeMnP/GNF	125	60	NF	platelet-like	[3]
Ni_2P–CoP	105	64	GCE	nanoparticles	[4]
NF-NiS_2	122	86	NF	nanosheets	[5]
NF-NiS_2-A	67	63	NF	nanosheets	
$Co_2P/Mo_2C/Mo_3Co_3C$@C	182	65	GCE	nanoparticles	[6]
$NiMo_2C$@C	169	30	GCE	nanoparticles with graphene layers.	[7]
Co_4Ni_1P NTs	129	52	GCE	nanotube	[8]
NFN-MOF/NF	87	35.2	NF	nanosheets	[9]
CoMn-S@NiO	232 (E_{100})	147.3	CC	nanosheets	[10]
$NiCoO_2$@C	128	61	NF	microflakes arrays	[11]
NG-Mo film	140.6	105	GCE	film	[12]
Ni_3Fe@N-CNT/ NF	76	98	GCE	nanofibers	[13]
CoP@NPCA-900 ($Zn_{0.80}Co_{0.20}$)	230	69.8	RDE	nanoparticles	[14]
Ni_2P–Cu_3P@NiCuC	78	177	NiCuC	nanoparticles	[15]
Pd-Co-NF	96	63	NF	nanofibers	This work
EA Pd-Co-NF@Pd NPs	57	55	NF	nanoparticles	This work

References

1 Drew, D.; Doyle, J. R.; Shaver, A. G. Cyclic Diolefin Complexes of Platinum and Palladium. *Inorg. Synth.*1972,*13,* 47-55.

2 Du, Y. M.; Li, Z. J.; Liu, Y. R.; Yang, Y.; Wang, L. Nickel-Iron Phosphides Nanorods Derived from Bimetallic-Organic Frameworks for Hydrogen Evolution Reaction. *Appl. Surface Sci.* **2018**, *457*, 1081-1086.

3 Zhao, Z. H.; Schipper, D. E.; Leitner, A. P.; Thirumalai, H.; Chen, J. H.; Xie, L. X.; Qin, F.; Alam, M. K.; Grabow, L. C.; Chen, S.; Wang, D. Z.; Ren, Z. F.; Wang, Z. M.; Whitmire, K. H.; Bao, J. M. Bifunctional Metal Phosphide FeMnP Films from Single Source Metal Organic Chemical Vapor Deposition for Efficient Overall Water Splitting. *Nano Energy* **2017**, *39*, 444-453.

4 Liang, X.; Zheng, B. X.; Chen, L. G.; Zhang, J. T.; Zhuang, Z. B.; Chen, B. H. MOF-Derived Formation of Ni_2P-CoP Bimetallic Phosphides with Strong Interfacial Effect toward Electrocatalytic Water Splitting. *ACS Appl. Mater. Interfaces* **2017**, *9*, 23222-23229.

5 Ma, Q. Y.; Hu, C. Y.; Liu, K. L.; Hung, S. F.; Ou, D. H.; Chen, H. M.; Fu,G.; Zheng, N. Identifying the Electrocatalytic Sites of Nickel Disulfide in Alkaline Hydrogen Evolution Reaction. *Nano Energy*

2017, *41*, 148-153.

6 Li, X.; Wang, X. L.; Zhou, J.; Han, L.; Sun, C. Y.; Wang, Q. W.; Su, Z. M. Ternary Hybrids as Efficient Bifunctional Electrocatalysts Derived from Bimetallic Metal–Organic-Frameworks for Overall Water Splitting. *J. Mater. Chem. A* **2018**, *6*, 5789-5796.

7 Li, X.; Yang, L.; Su, T.; Wang, X. L.; Sun, C. Y.; Su, Z. M. Graphene-Coated Hybrid Electrocatalysts Derived from Bimetallic Metal–Organic Frameworks for Efficient Hydrogen Generation. *J. Mater. Chem. A* **2017**, *5*, 5000-5006.

8 Yan, L. T.; Cao, L.; Dai, P. C.; Gu, X.; Liu, D. D.; Li, L. J.; Wang, Y.; Zhao, X. B. Metal-Organic Frameworks Derived Nanotube of Nickel-Cobalt Bimetal Phosphides as Highly Efficient Electrocatalysts for Overall Water Splitting. *Adv. Funct. Mater.* **2017**, *27,* 1703455.

9 Raja, D. S.; Chuah, X. F.; Lu, S. Y. In Situ Grown Bimetallic MOF-Based Composite as Highly Efficient Bifunctional Electrocatalyst for Overall Water Splitting with Ultrastability at High Current Densities. *Adv. Energy Mater.* **2018**, *8*, 1801065.

10 Li, Q.; Xing, Z. C.; Wang, D. W.; Sun, X. P. ; Yang, X. R. In Situ Electrochemically Activated CoMn-S@NiO/CC Nanosheets Array for Enhanced Hydrogen Evolution. *ACS Catal.* **2016***, 6,* 2797−2801.

11 Yin, X. C.; Sun, G.; Su, L.; Wang, L. X.; Shao, G. J. Surface Roughening of Nanoparticle-Stacked Porous $NiCoO_2$@C Microflakes Arrays Grown on Ni Foam for Enhanced Hydrogen Evolution Activity. *Electrochimica Acta* **2018**, *284*, 226–233.

12 Chen, S.; Duan, J. J.; Tang, Y. H.; Jin, B.; Qiao, S. Z. Molybdenum Sulfide Clusters-Nitrogen-Doped Graphene Hybrid Hydrogel Film as an Efficient Three-Dimensional Hydrogen Evolution Electrocatalyst. *Nano Energy* **2015**, *11*, 11–18.

13 Li, T. F.; Luo, G.; Liu, K. H.; Li, X.; Sun, D. M.; Xu, L.; Li, Y. F. ; Tang, Y. W. Encapsulation of Ni3Fe Nanoparticles in N-Doped Carbon Nanotube-Grafted Carbon Nanofibers as High-Efficiency Hydrogen Evolution Electrocatalysts. *Adv. Funct. Mater.* **2018**, *28*, 1805828.

14 Guo, H.; Feng, Q.; Xu, K.; Xu, J.; Zhu, J.; Zhang, C.; Liu, T. Self-Templated Conversion of Metallogel into Heterostructured TMP@Carbon Quasiaerogels Boosting Bifunctional Electrocatalysis. *Adv. Funct. Mater.* **2019**, *29*, 1903660.

15 Yu, L.; Zhang, J.; Dang, Y.; He, J.; Tobin, Z.; Kerns, P.; Dou, Y.; Jiang, Y.; He, Y.; Suib, S. L., In Situ Growth of Ni_2P–Cu_3P Bimetallic Phosphide with Bicontinuous Structure on Self-Supported NiCuC Substrate as an Efficient Hydrogen Evolution Reaction Electrocatalyst. *ACS Catal.* **2019**, *9*, 6919-6928.

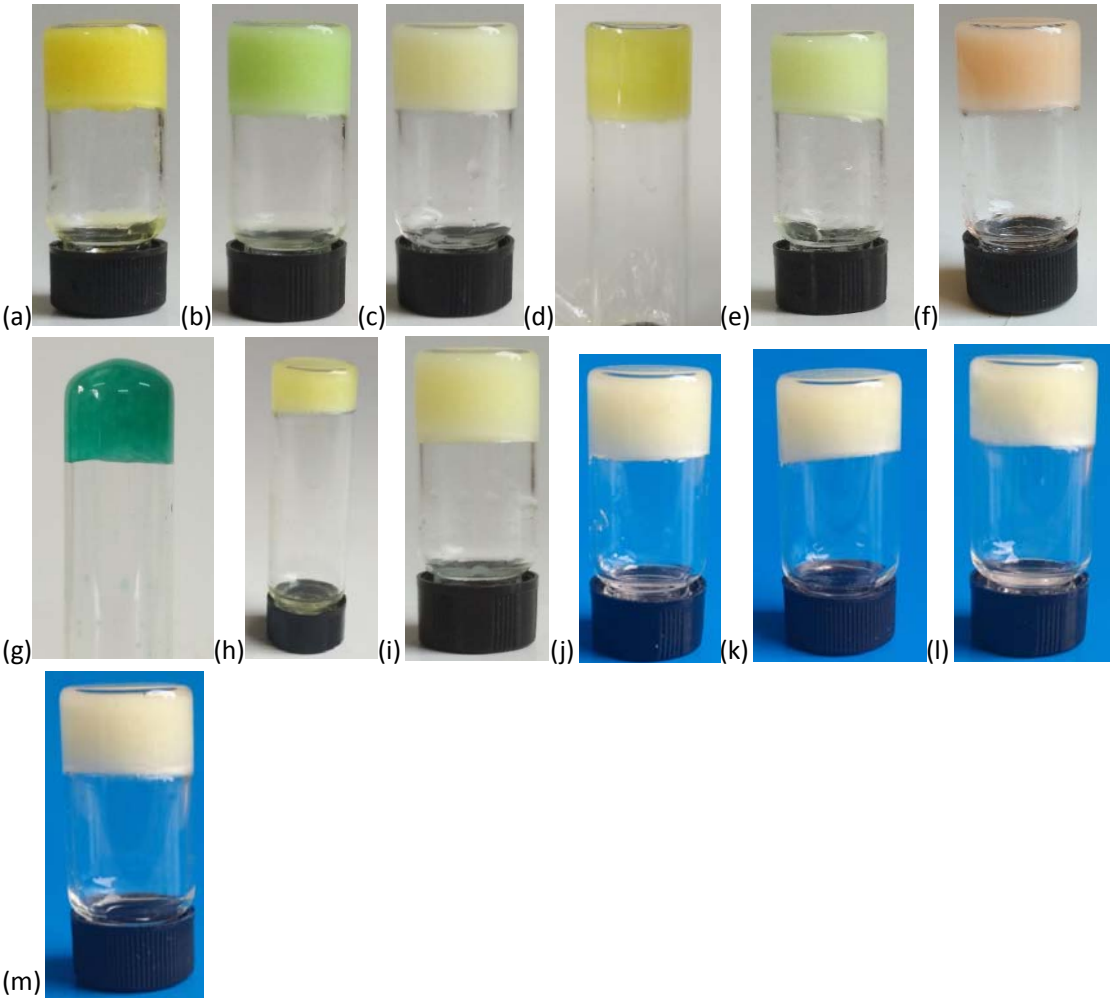

Figure S1. Photographic images of various metal-organic gels, (a) **Pd-Fe** (Cl^-), (b) **Pd-Cu** (Cl^-), (c) **Pd-Zn** (Cl^-), (d) **Pd-Ni** (NO_3^-), (e) **Pd-Ni** (Cl^-), (f) **Pd-Co** (NO_3^-), (g) **Pd-Co** (Cl^-), (h) **Pd-Mn** (NO_3^-), (i) **Pd-Mn** (Cl^-) and rare earth metal gels (j) **Pd-Y** (NO_3^-), (k) **Pd-Tb** (NO_3^-), (l) **Pd-Ce** (NO_3^-), (m) **Pd-La** (NO_3^-).

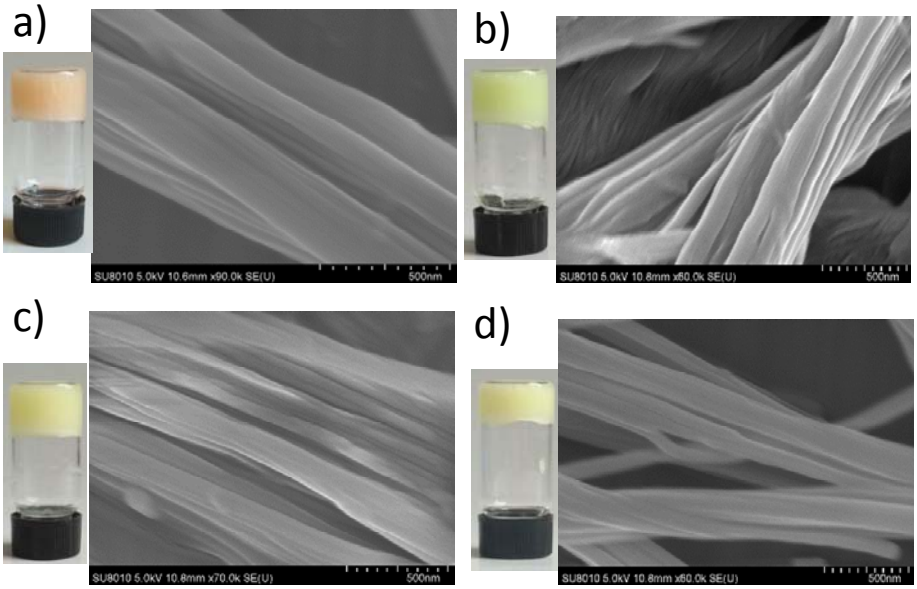

Figure S2. Photographic images of (a) **Pd-Co** (NO_3^-), (b) **Pd-Ni** (Cl^-), (c) **Pd-Mn** (Cl^-) and (d) **Pd** metal-organic gels and SEM images of the corresponding xerogels.

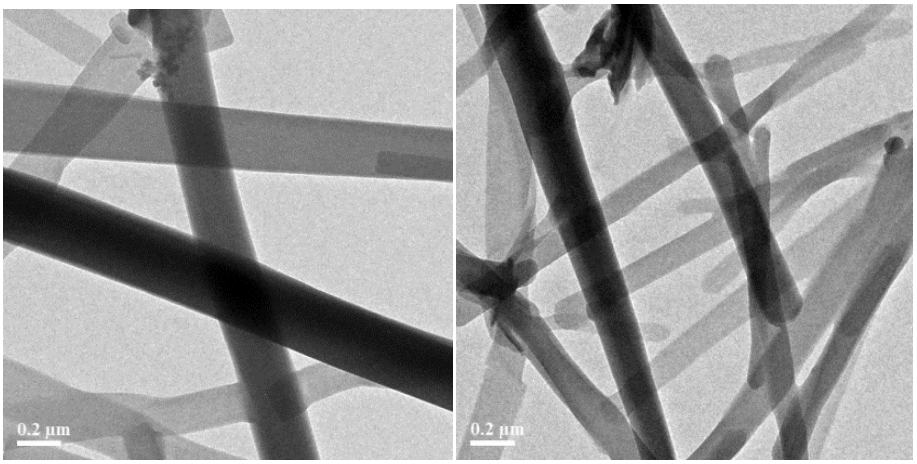

Figure S3. TEM images of **Pd-Ni** xerogel.

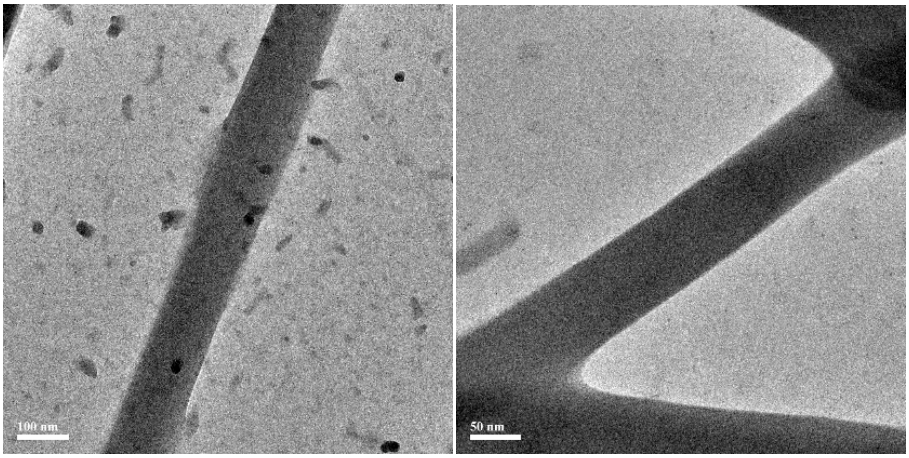

Figure S4. TEM images of **Pd-Mn** xerogel.

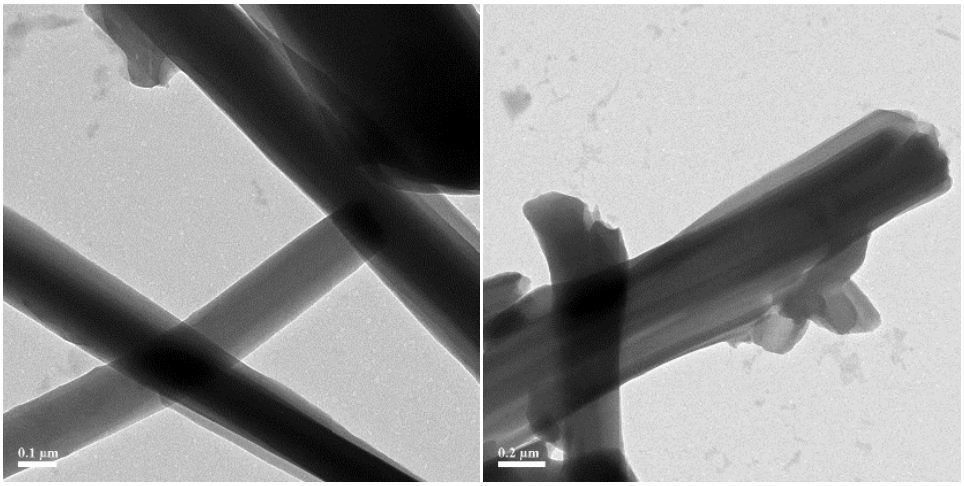

Figure S5. TEM images of **Pd** xerogel.

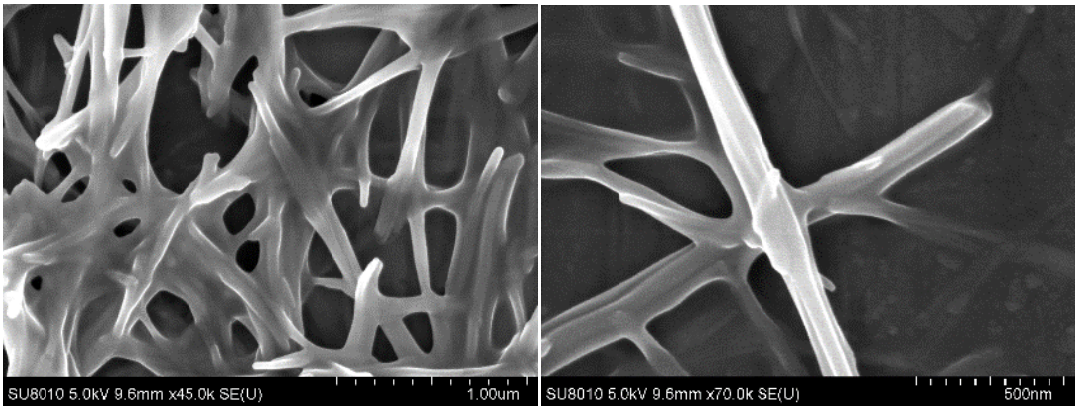

Figure S6. SEM images of **Pd-Cu** xerogel.

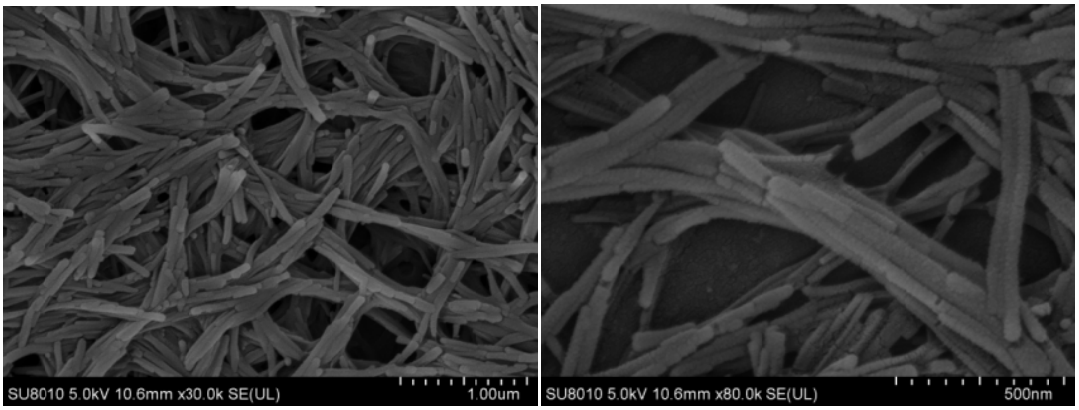

Figure S7. SEM images of **Pd-Zn** xerogel.

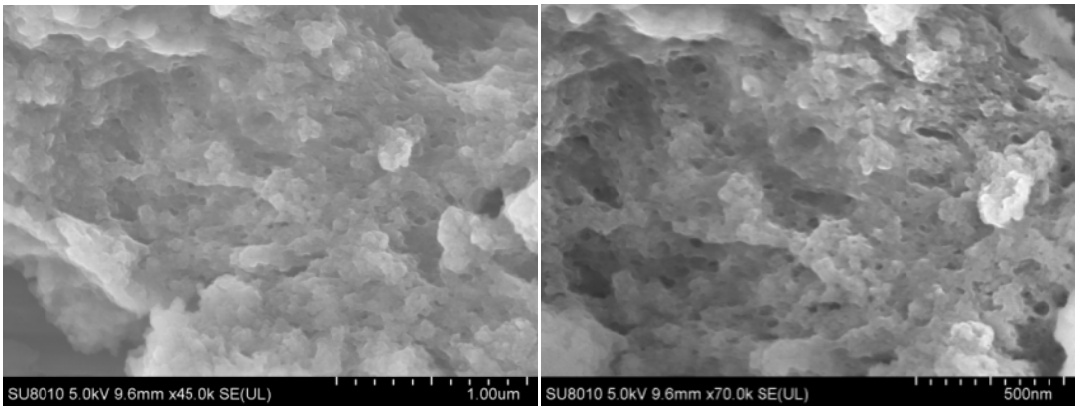

Figure S8. SEM images of **Pd-Al** xerogel.

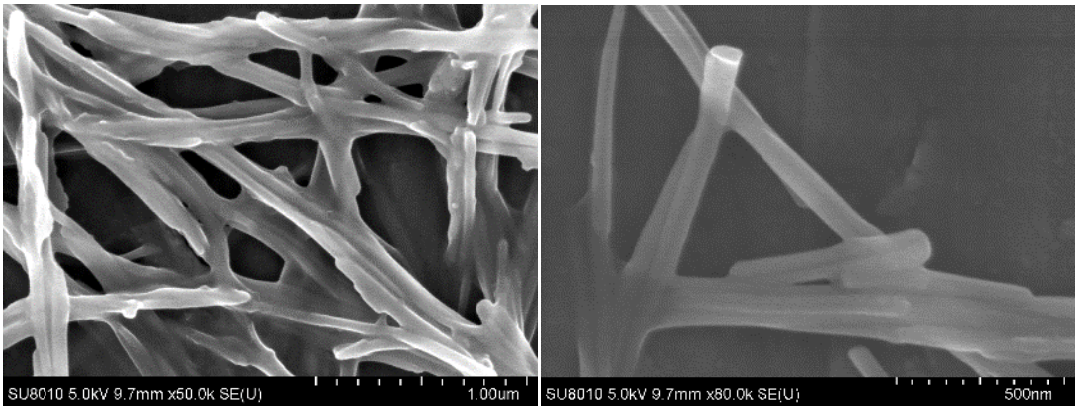

Figure S9. SEM images of **Pd-Fe** xerogel.

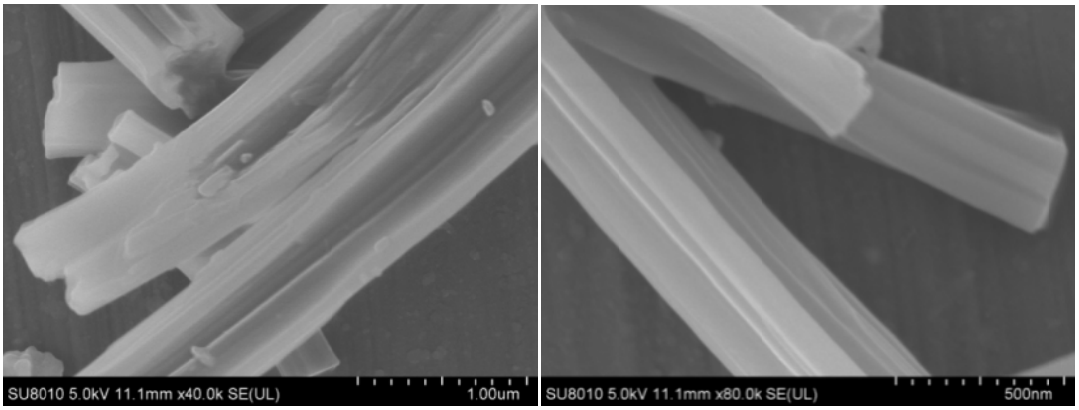

Figure S10. SEM images of **Pd-Y** xerogel.

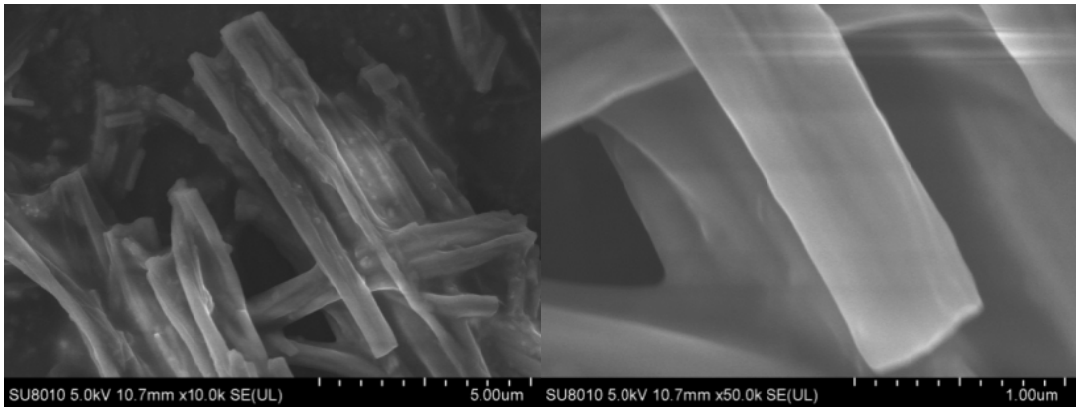

Figure S11. SEM images of **Pd-La** xerogel.

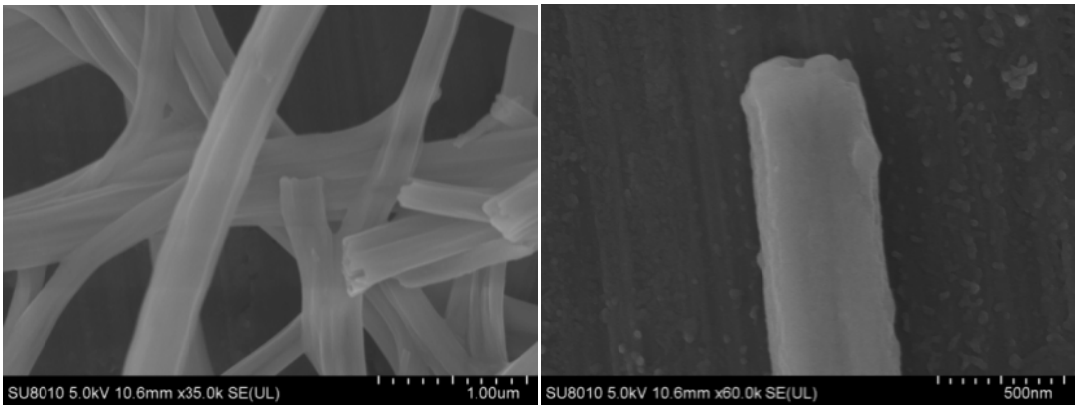

Figure S12. SEM images of **Pd-Ce** xerogel.

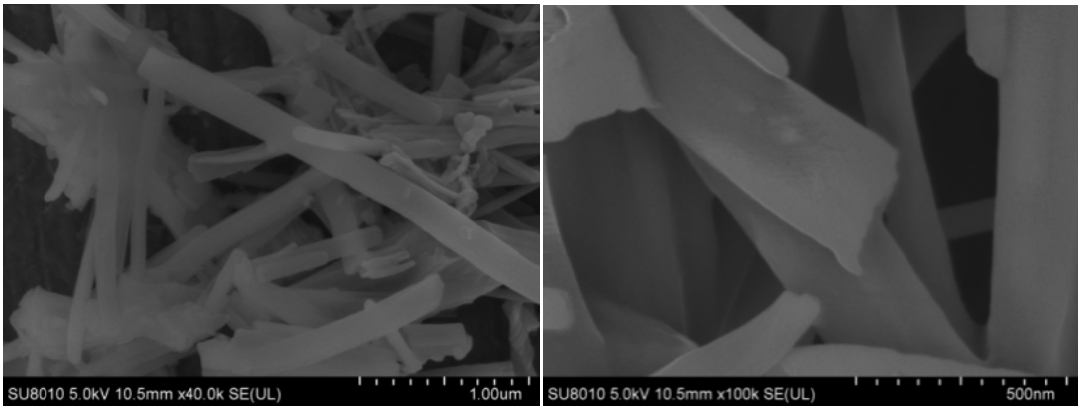

Figure S13. SEM images of **Pd-Tb** xerogel.

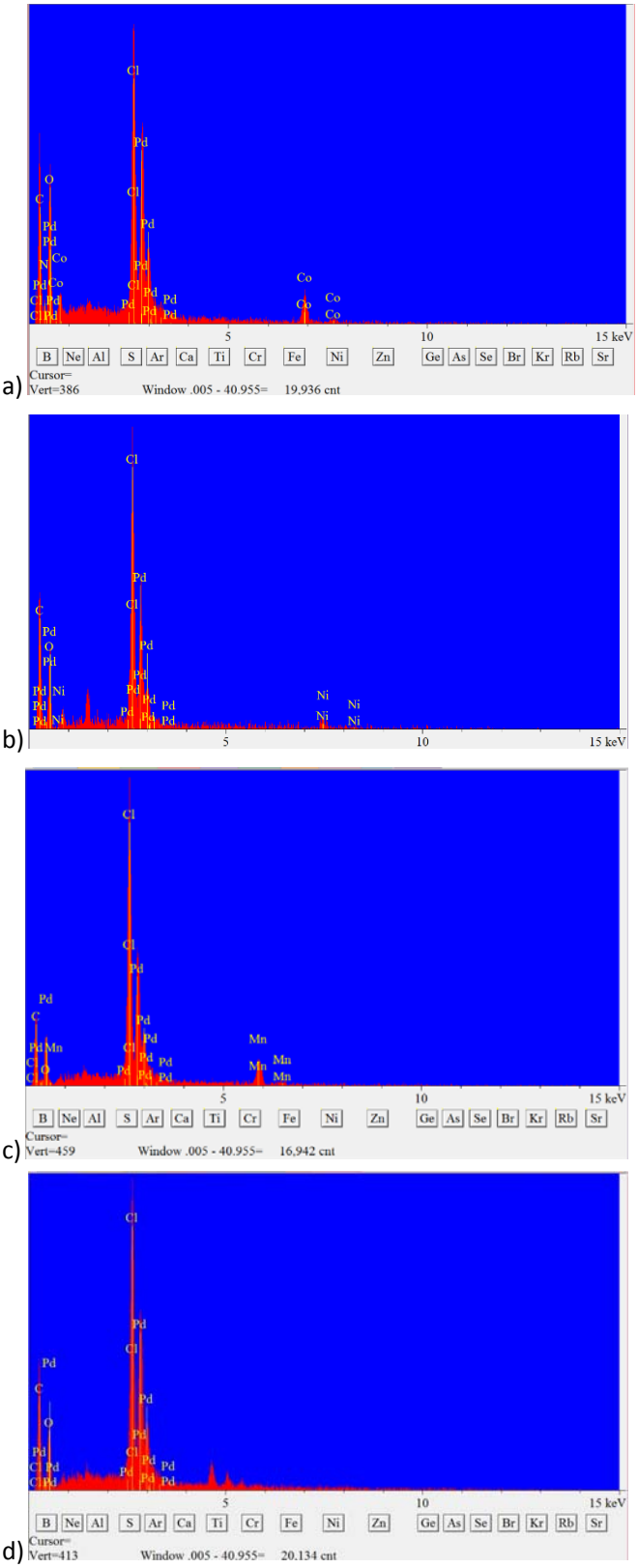

Figure S14. EDX spectra of **Pd-Co** (Quantitative value/atom%: Pd 6.745, Co 2.211, Cl 7.342), **Pd-Ni** (Quantitative value/atom%: Pd 5.454, Ni 1.333, Cl 8.309), **Pd-Mn** (Quantitative value/atom%: Pd6.256, Mn 2.971, Cl 13.057), and **Pd** xerogels (Quantitative value/atom%: Pd 4.833, Cl 4.961).

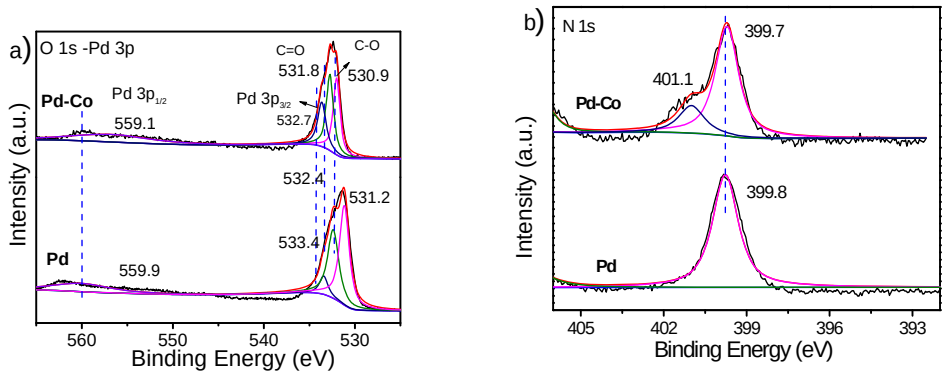

Figure S15. XPS survey spectrum of (a) O 1s –Pd 3p and (b) N 1s spectra of **Pd-Co** and **Pd** xerogels.

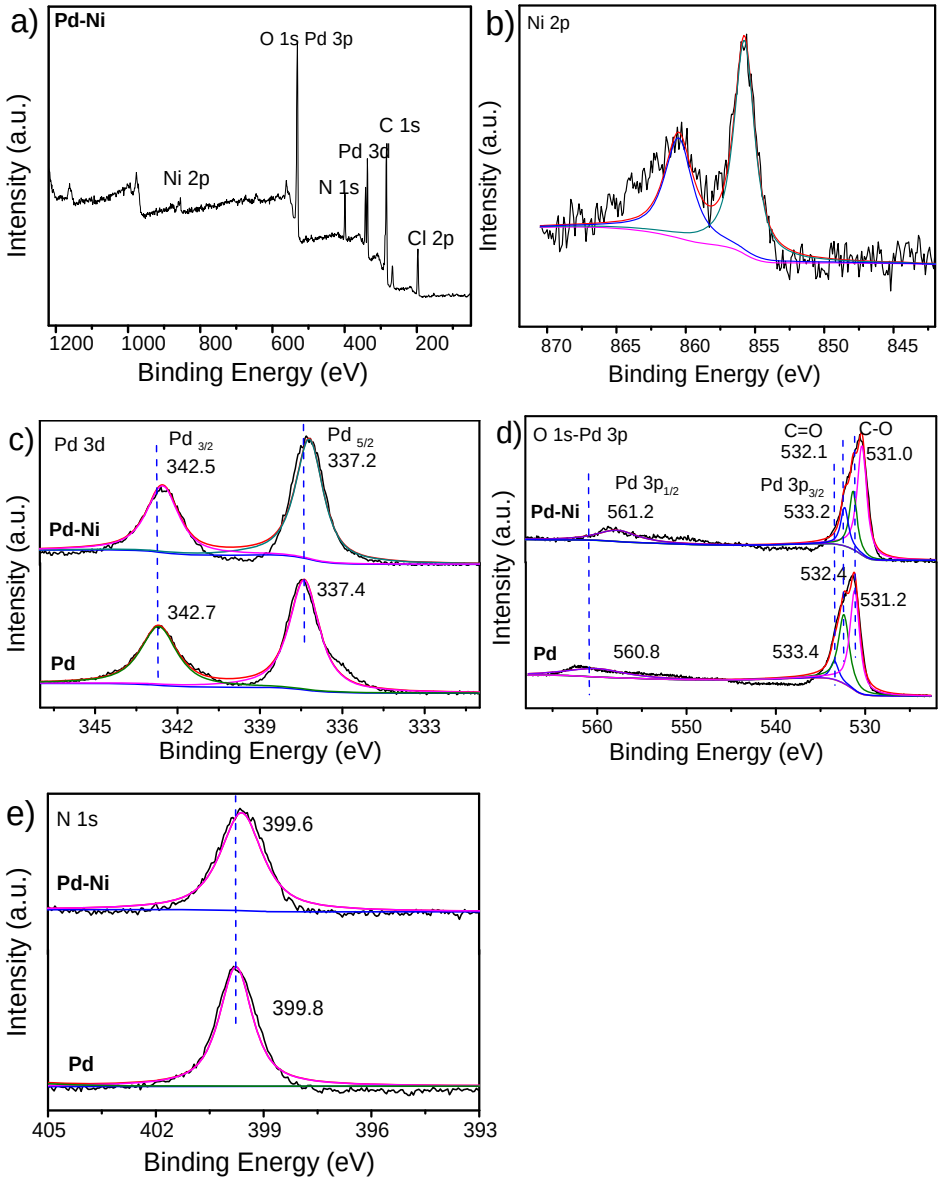

Figure S16. XPS survey spectrum of **Pd-Ni** xerogel (a) survey, (b) Ni 2p, (c) Pd 3d, (d) O 1s –Pd 3p, (e) N 1s.

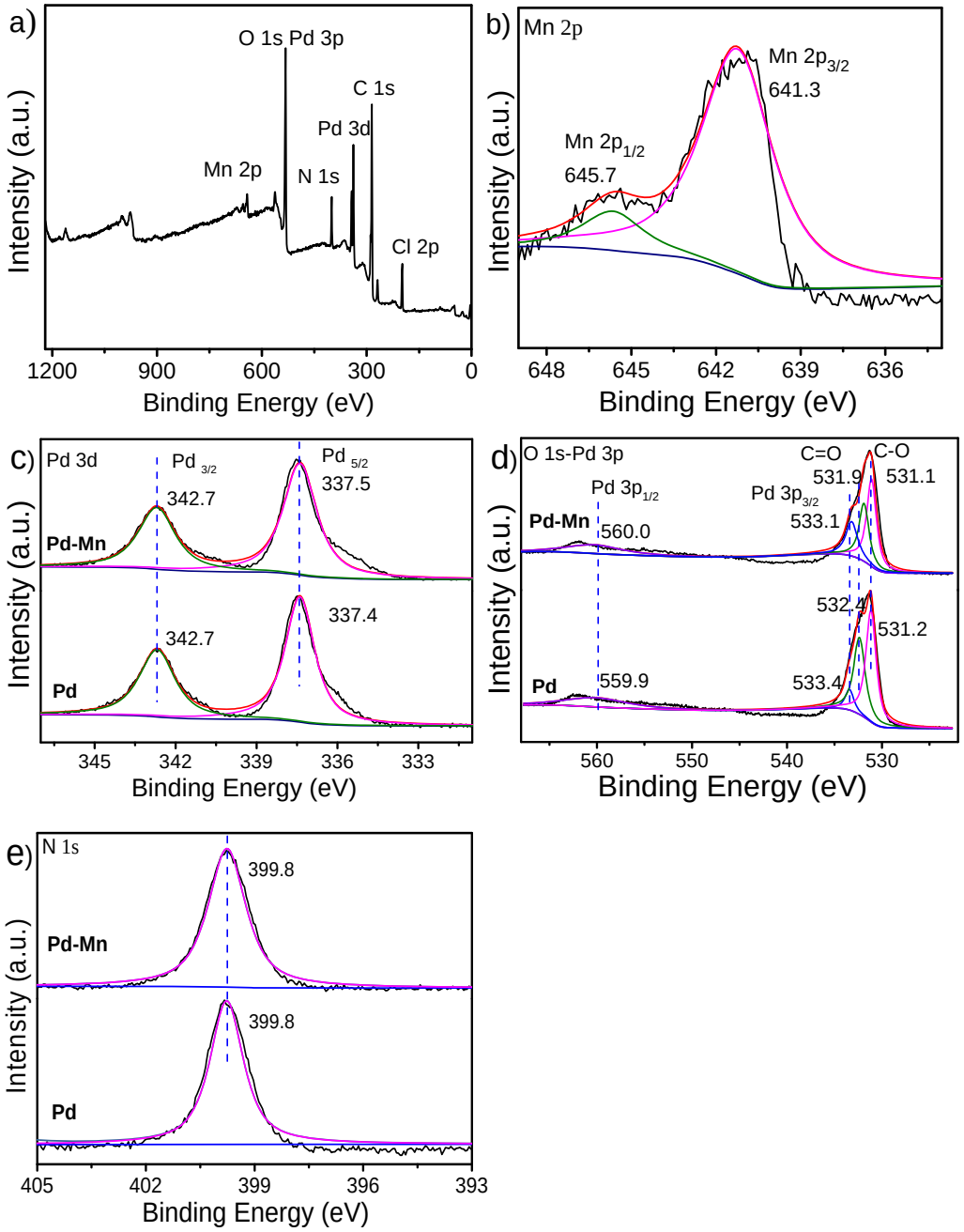

Figure S17. XPS survey spectrum of **Pd-Mn** xerogel (a) survey, (b) Mn 2p, (c) Pd 3d, (d) O 1s –Pd 3p, (e) N 1s.

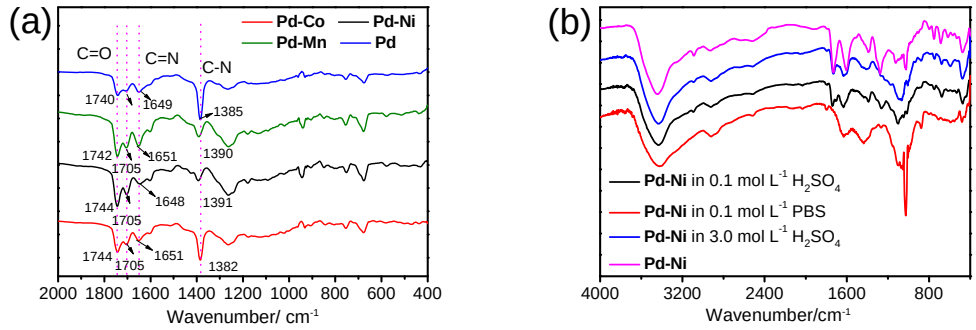

Figure S18. FT-IR spectra of (a) **Pd-Co**, **Pd-Ni**, **Pd-Mn** and **Pd**, and (b) **Pd-Ni** xerogel in acidic and basic solutions.

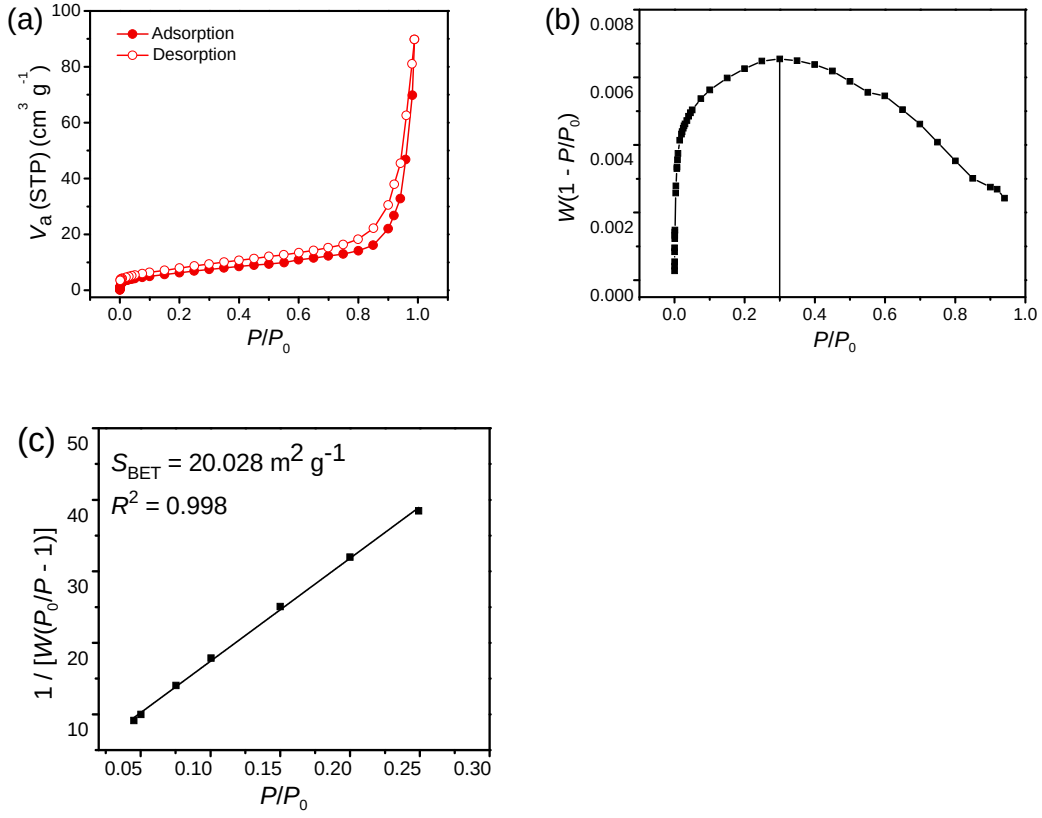

Figure S19. a) N_2 adsorption (closed symbols) /desorption (open symbols) isotherms at 77 K, b) BET fit, and c) consistency plot for **Pd-Co** xerogel.

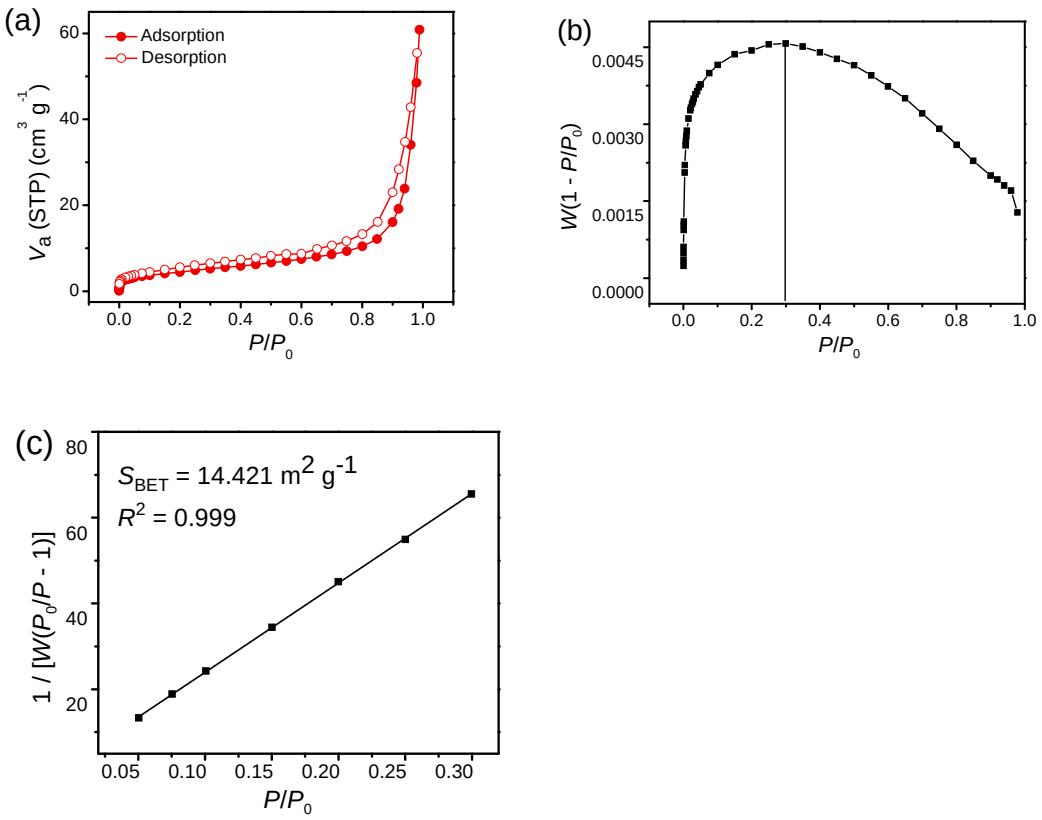

Figure S20. a) N_2 adsorption (closed symbols) /desorption (open symbols) isotherms at 77 K, b) BET fit, and c) consistency plot for **Pd-Ni** xerogel.

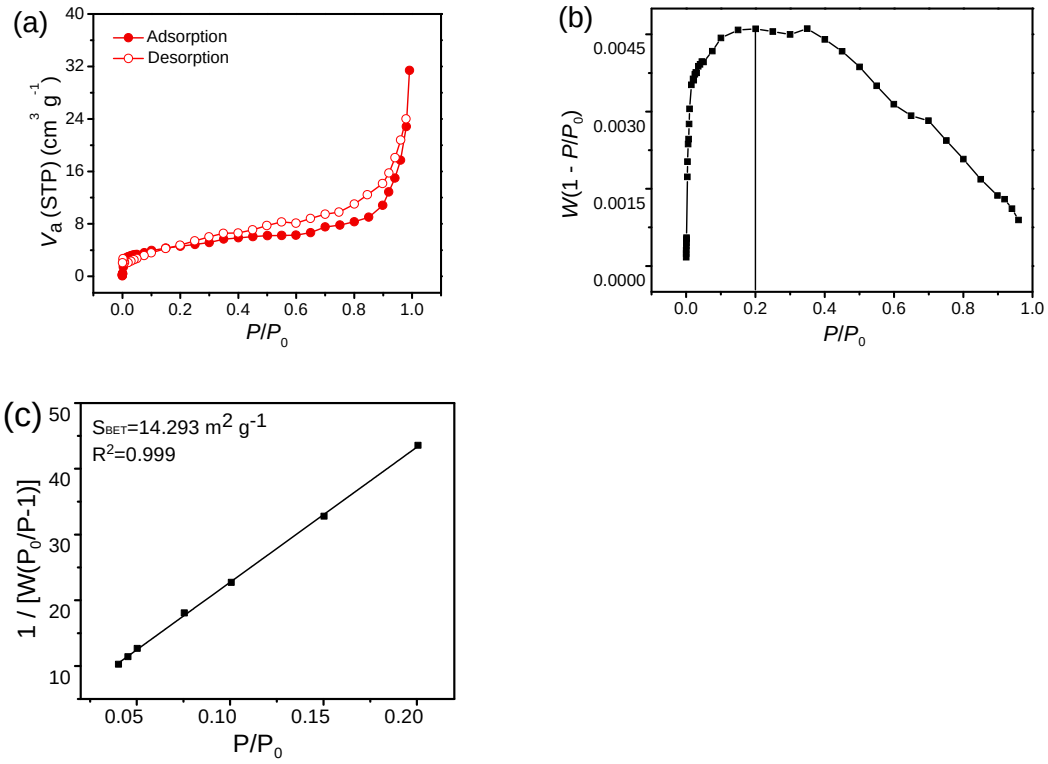

Figure S21. a) N_2 adsorption (closed symbols) /desorption (open symbols) isotherms at 77 K, b) BET fit, and c) consistency plot for **Pd-Mn** xerogel.

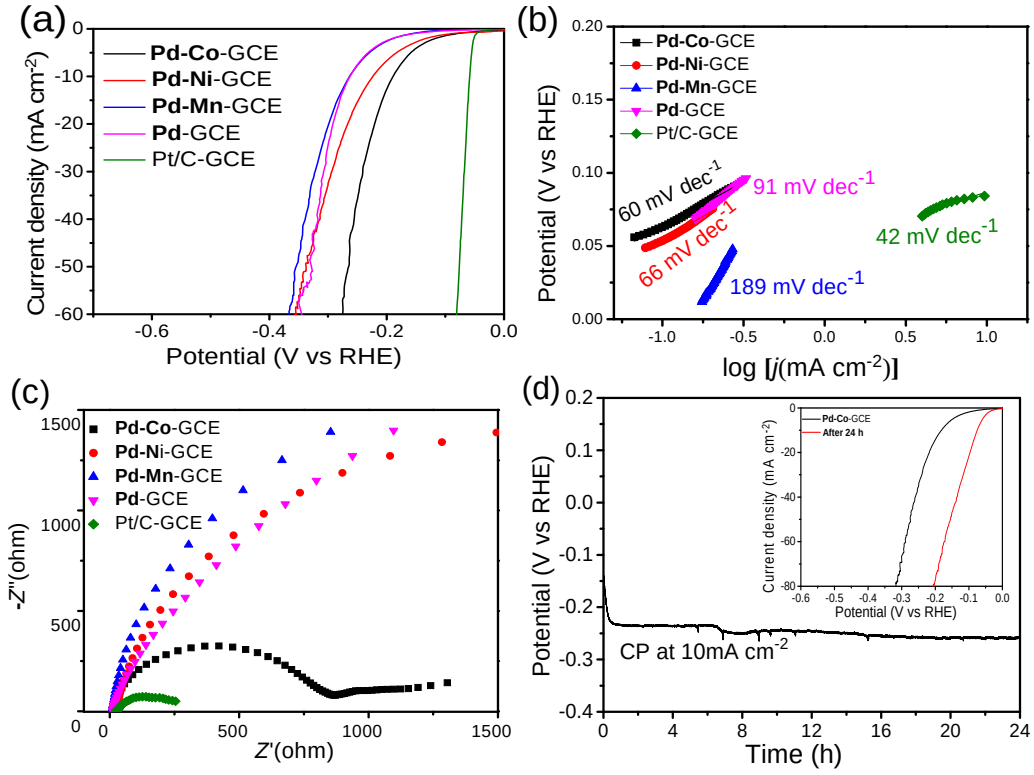

Figure S22. Electrochemical performances of bimetallic **Pd-Co**, **Pd-Ni**, **Pd-Mn**, and homometallic **Pd** nanofiber xerogels and Pt/C loaded on GCE, (a) LSV polarization curves by area normalization method, (b) Tafel plots, (c) EIS Nyquist plots, (d) Chronopotentiometric curve of **Pd-Co-NF** in 0.5 mol L^{-1} H_2SO_4 electrolyte at a fixed current density of 10 mA cm^{-2}, (Inset) comparison of LSV polarization curves of **EA Pd-Co-NF** before and after 24 h.

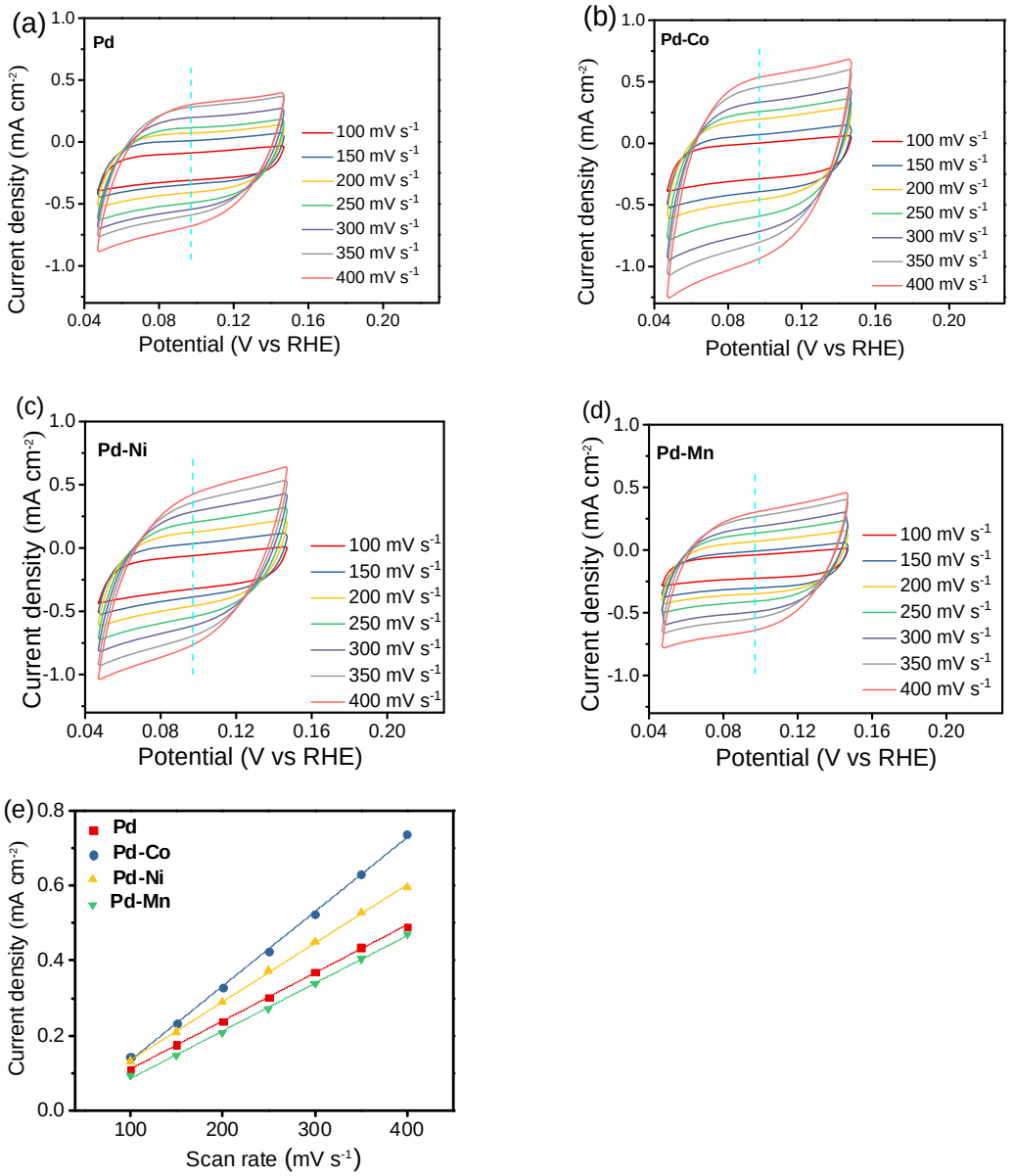

Figure S23. CV curves and fitting linear of heterometallic gel with different scan rates for (a) **Pd-Co**, (b) **Pd-Ni**, (c) **Pd-Mn** and (d) **Pd**, and (e) linear fitting of Δ_j ($\Delta_j = j_a - j_c$) vs. scan rates at a given overpotential of +0.097 V vs. RHE in 0.5 mol L^{-1} H_2SO_4.

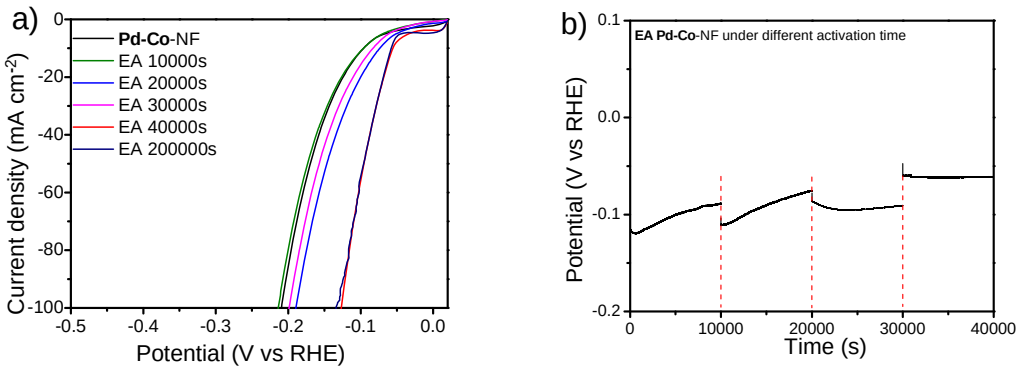

Figure S24. (a) LSV plots for **EA Pd-Co@Pd NPs** and **Pd-Co** loading on NF after 40000 s, and (b) Chronopotentiometry activation of **Pd-Co**-NF under different activation time at current density of 10 mA cm^{-2}.

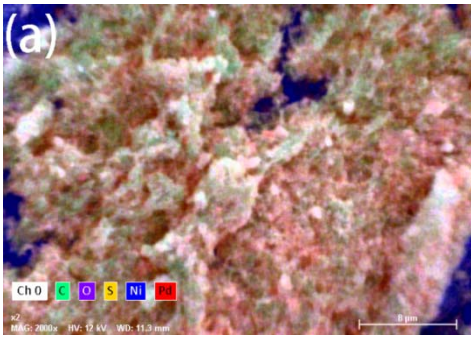

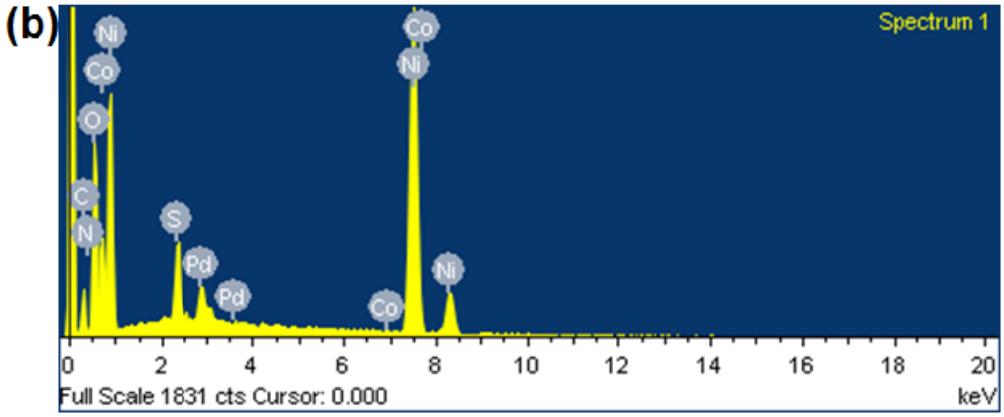

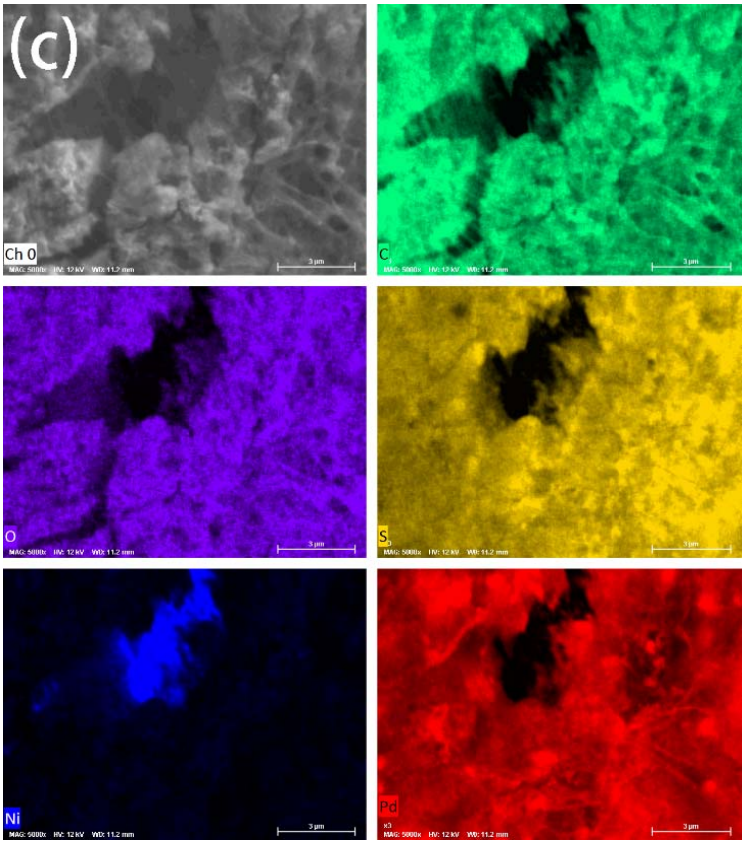

Figure S25. a,b) EDX spectrum of **EA Pd-Co@Pd NPs** (Quantitative value/atom%: Pd 0.86, Co 0, Ni 54.01, S 2.32) and c) elemental mapping images of C, N, O, Pd, Co element mappings.

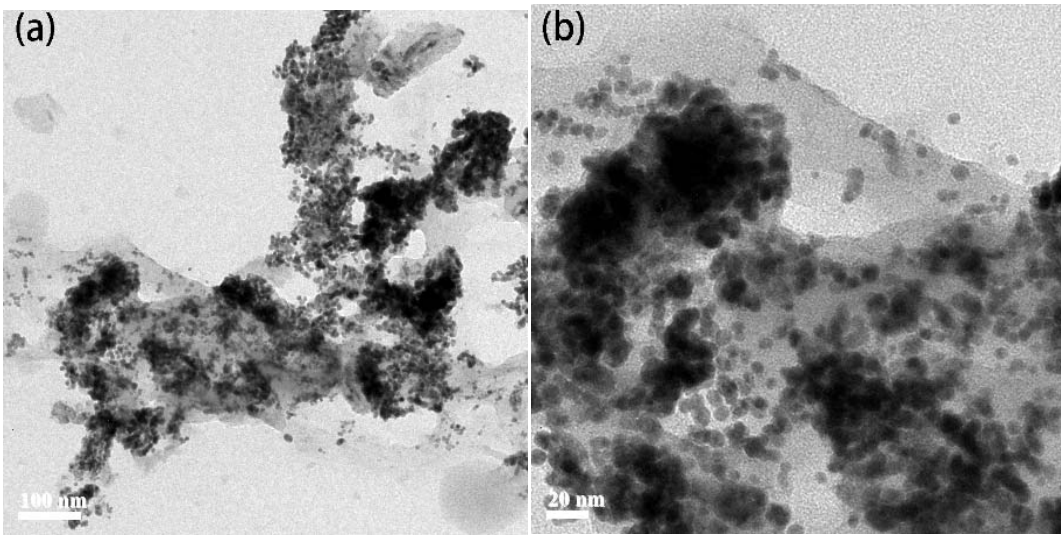

Figure S26. TEM images of **EA Pd-Co@Pd NPs** placed at room temperature for two weeks.

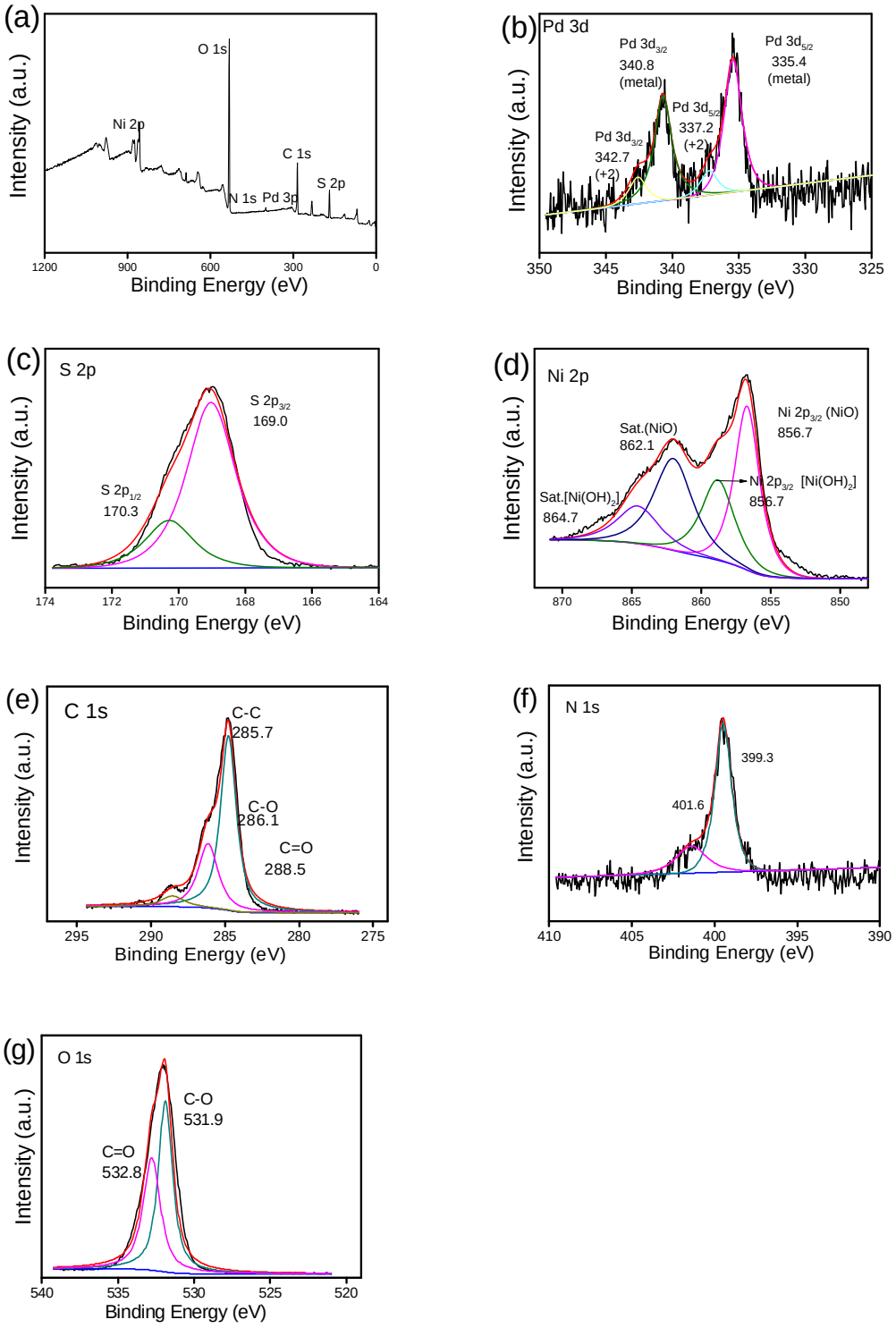

Figure S27. XPS spectra of **EA Pd-Co@Pd NPs**, a) survey, b) Pd 3d, c) S 2p, d) Ni 2p, e) C 1s, f) O 1s, g) N 1s.

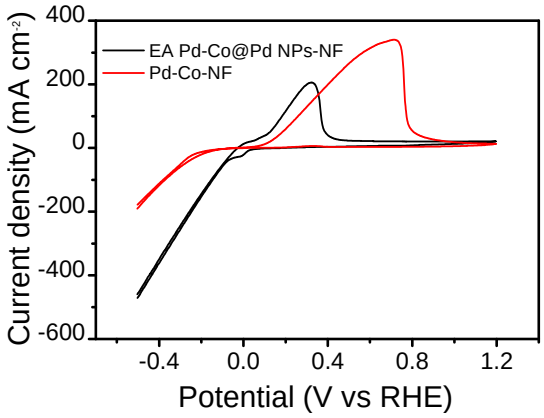

Figure S28. CV curves of **Pd-Co** and **EA Pd-Co@Pd NPs** at scan rate of 20 mV s^{-1} in 0.5 mol L^{-1} H_2SO_4 solution.

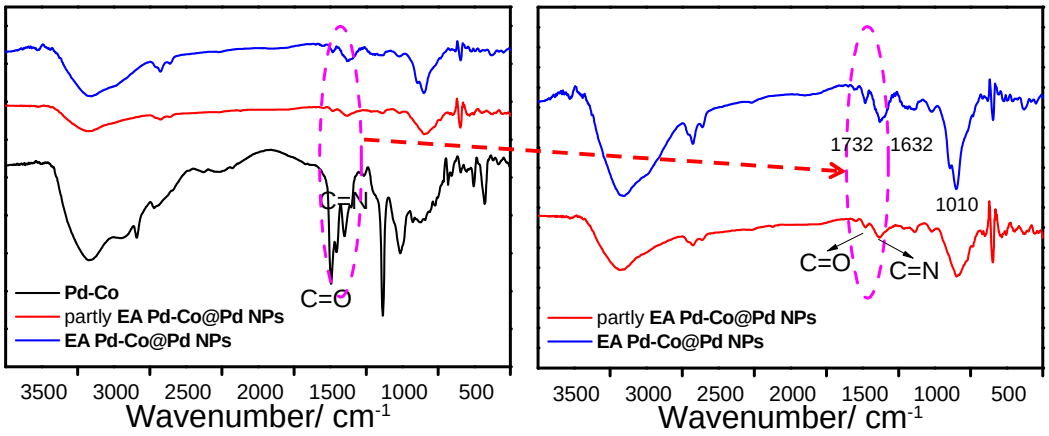

Figure S29. FT-IR spectra of **Pd-Co**, **EA Pd-Co@Pd NPs** after 80 h and partly **EA Pd-Co@Pd NPs** after 20 cyclic voltammograms cycles.